GRAVITATION

Lense–Thirring frame dragging induced by a fast-rotating white dwarf in a binary pulsar system

V. Venkatraman Krishnan[1,2]*, M. Bailes[1,3], W. van Straten[4], N. Wex[2], P. C. C. Freire[2], E. F. Keane[1,5], T. M. Tauris[6,7,2], P. A. Rosado[1]†, N. D. R. Bhat[8], C. Flynn[1], A. Jameson[1], S. Osłowski[1]

Radio pulsars in short-period eccentric binary orbits can be used to study both gravitational dynamics and binary evolution. The binary system containing PSR J1141–6545 includes a massive white dwarf (WD) companion that formed before the gravitationally bound young radio pulsar. We observed a temporal evolution of the orbital inclination of this pulsar that we infer is caused by a combination of a Newtonian quadrupole moment and Lense–Thirring (LT) precession of the orbit resulting from rapid rotation of the WD. LT precession, an effect of relativistic frame dragging, is a prediction of general relativity. This detection is consistent with an evolutionary scenario in which the WD accreted matter from the pulsar progenitor, spinning up the WD to a period of <200 seconds.

In general relativity (GR), the mass–energy current of a rotating body induces a gravitomagnetic field, so called because it has formal similarities with the magnetic field generated by an electric current (*1*). This gravitomagnetic interaction drags inertial frames in the vicinity of a rotating mass. The strength of this drag is proportional to the body's intrinsic angular momentum (spin). Frame dragging in a binary system causes a precession of the orbital plane called Lense–Thirring (LT) precession (*2*). The effect has been detected in the weak-field regime by satellite experiments in the gravitational field of the rotating Earth (*3*, *4*). Frame dragging is also a plausible interpretation for x-ray spectra of accreting black holes because it affects photon propagation and the properties of the accretion disk, which in some cases allows the determination of the black hole spin (*5*).

In binary pulsar systems [systems containing both a rotating magnetized neutron star (NS), the radio emission of which is visible from Earth as a pulsar, and an orbiting companion star], relativistic frame dragging caused by the spin of either the pulsar or its companion is expected to contribute to spin–orbit coupling. These relativistic effects are seen in addition to Newtonian contributions from a mass-quadrupole moment (QPM) induced by the rotation of the body (*6*). Both contributions cause precession of the position of the periastron (ω; the point in the pulsar orbit that is closest to its companion) and precession of the orbital plane, changing the orbital inclination (*i*; see Fig. 1). If these precessional effects are induced by the NS rotation, then they are dominated by LT, whereas in the case of a rotating main-sequence companion star, they are dominated by QPM interactions (*6*, *7*). Fast-rotating white dwarf (WD) companions with spin periods of a few minutes fall between

[1]Centre for Astrophysics and Supercomputing, Swinburne University of Technology, Melbourne, Victoria 3122, Australia. [2]Max-Planck-Institut für Radioastronomie, D-53121 Bonn, Germany. [3]Australian Research Council Centre of Excellence for Gravitational Wave Discovery (OzGrav), Swinburne University of Technology, Melbourne, Victoria 3122, Australia. [4]Institute for Radio Astronomy and Space Research, Auckland University of Technology, Auckland 1142, New Zealand. [5]Square Kilometer Array Organisation, Jodrell Bank Observatory, Macclesfield SK11 9DL, UK. [6]Aarhus Institute of Advanced Studies, Aarhus University, 8000 Aarhus C, Denmark. [7]Department of Physics and Astronomy, Aarhus University, 8000 Aarhus C, Denmark. [8]International Centre for Radio Astronomy Research, Curtin University, Bentley, Western Australia 6102, Australia.
***Corresponding author. Email: vkrishnan@mpifr-bonn.mpg.de**
†Present address: Holaluz-Clidom S.A., Passeig de Joan de Borbó 99-101, 4a Planta, 08039 Barcelona, Spain.

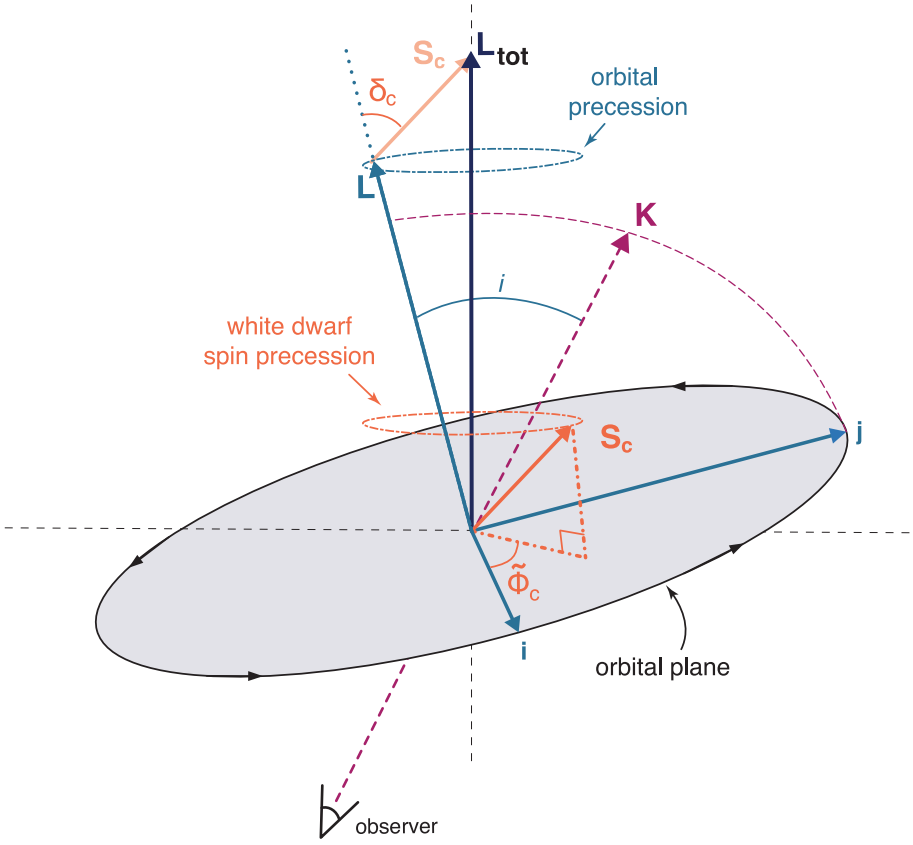

Fig. 1. Definition of the orbital geometry. Diagram illustrating the orbital geometry of the system following the "DT92" convention (*10*) with all vectors shifted to the origin. **L** is the angular momentum of the orbit, which is perpendicular to the orbital plane and inclined at an angle *i* to the line-of-sight vector, **K**. The plane containing the vectors **L** and **K** intersects the orbital plane, defining the orbital plane's unit vector **j** and its perpendicular counterpart **i**. $\mathbf{S}_c$ is the spin angular momentum of the WD companion, which is misaligned from **L** by an angle δ_c. The vector sum of **L** and $\mathbf{S}_c$ forms the total angular momentum vector $\mathbf{L}_{tot}$, which is invariant, whereas **L** and $\mathbf{S}_c$ precess. $\tilde{\Phi}_c$ is the angle that the projection of $\mathbf{S}_c$ on the orbital plane subtends with respect to **i** and is related to the precession phase of the WD (Φ_c) as $\tilde{\Phi}_c = \Phi_c - 270°$. The precessions of **L** and $\mathbf{S}_c$ form precession cones around $\mathbf{L}_{tot}$ as labeled. The precession of $\mathbf{S}_c$ causes Φ_c to sweep through 360°, whereas its rate of advance is modulated by the precession of **L**, which induces small oscillations to the position of **j** and thus in **i**. Some angles and vector magnitudes in the figure are exaggerated for clarity. In practice, $|\mathbf{L}| >> |\mathbf{S}_c|$; even if the WD is spinning at its breakup speed, the angle between **L** and $\mathbf{L}_{tot}$ is at most 0.74°. A more detailed version of this diagram is shown in fig. S1.

these two extremes and are expected to yield similar contributions from both effects (*8*). Although QPM spin–orbit interaction has already been observed in some binary pulsars [e.g., PSR J0045–7319 (*7*)], no binary pulsar orbit has been shown to experience a measurable contribution from LT drag.

The times of arrival (TOAs) of the radio pulses from pulsars can be measured with high precision, with uncertainties that are often more than three orders of magnitude smaller than their spin periods. This allows pulsars to be monitored for decades without losing rotational phase information. This "pulsar-timing" methodology can provide precise measurements of the pulsar's spin and astrometric parameters (*9*). For pulsars in binary systems, pulsar timing also provides precise measurements of the binary orbit: five parameters describing the nonrelativistic (Keplerian) parameters and, for some binaries, relativistic effects that affect both the orbit and the propagation of the radio signals (*10*). These relativistic effects are typically parameterized using theory-independent post-Keplerian (PK) parameters (*11*, *12*). Measurements of two PK parameters can be used to obtain the mass of the pulsar (M_p) and of the companion (M_c) by assuming a theory of gravity, such as GR, whereas three or more PK parameters can be used to perform self-consistency tests of that theory. An alternative formalism assumes a theory of gravity such as GR, which allows direct model fitting of the component masses. The latter is preferred if the goal is to understand the properties and dynamics of the system under that theory, rather than testing the theory itself. We adopt this approach and assume that GR adequately describes the system.

PSR J1141–6545 is a radio pulsar with a spin period of ~394 ms in an ~4.74-hour eccentric orbit with a massive WD companion (*13*, *14*). It is one of only two confirmed NS–WD binary systems (the other being PSR B2303+46, a much wider-orbit binary) in which the WD is known to have formed first and is thus older than the NS. This requires an unusual evolution of the stellar pair (*15*, *16*). The initially more massive (primary) star must have formed the older massive WD. Forming a NS requires a higher stellar mass, so the initially (slightly) less massive secondary star must have accreted sufficient mass from the primary star to explode in a supernova (SN), producing the pulsar. Before exploding, the secondary would have undergone an expansion leading to mass transfer back to the primary star, by that point already a WD.

Because the primary was already a WD, there cannot have been subsequent mass accretion onto the newly formed pulsar. Thus, unlike most other pulsars with WD companions, PSR J1141–6545 and PSR B2303+46 were not spun up by mass transfer; they still have the large magnetic field strengths typical of young pulsars, as inferred from their spin evolution. The pulsar spin axes, which are expected to have started at a random orientation with respect to the orbital plane after the SN explosion, were therefore not aligned with the orbital angular momentum by an accretion process. For a compact system, such a misalignment can result in observable relativistic spin precession of the pulsar (*17*). This has been observed in PSR J1141–6545 as precession led to temporal evolution of the pulse profile, providing constraints on the system's geometry (*18*, *19*).

PSR J1141–6545 has been observed since 2000, allowing the determination of several PK parameters including the advance of periastron ($\dot{\omega}$), relativistic time dilation, gravitational wave damping, and the Shapiro delay. These are all in agreement with GR (*8*), justifying our assumption of the theory. We seek the measurement of an additional PK parameter, the temporal evolution of the observed projected semimajor axis (x_{obs}), which to necessary precision can be written as $x_{obs} = (a_p \sin i/c) + A$, where a_p is the semimajor axis of the pulsar's orbit, i its inclination, c is the speed of light, and A is the first "aberration" parameter, which describes how the aberration of the pulsar signal affects our measurement of x (*8*, *10*).

Timing observations of PSR J1141−6545 have been undertaken using the 64-m Parkes and the UTMOST radio telescopes (*20*). Our data recording and TOA extraction followed standard pulsar data acquisition and reduction methods (*8*). The timing data were analyzed using the DDGR model (*21*), which describes the timing of the pulsar using GR. The measured

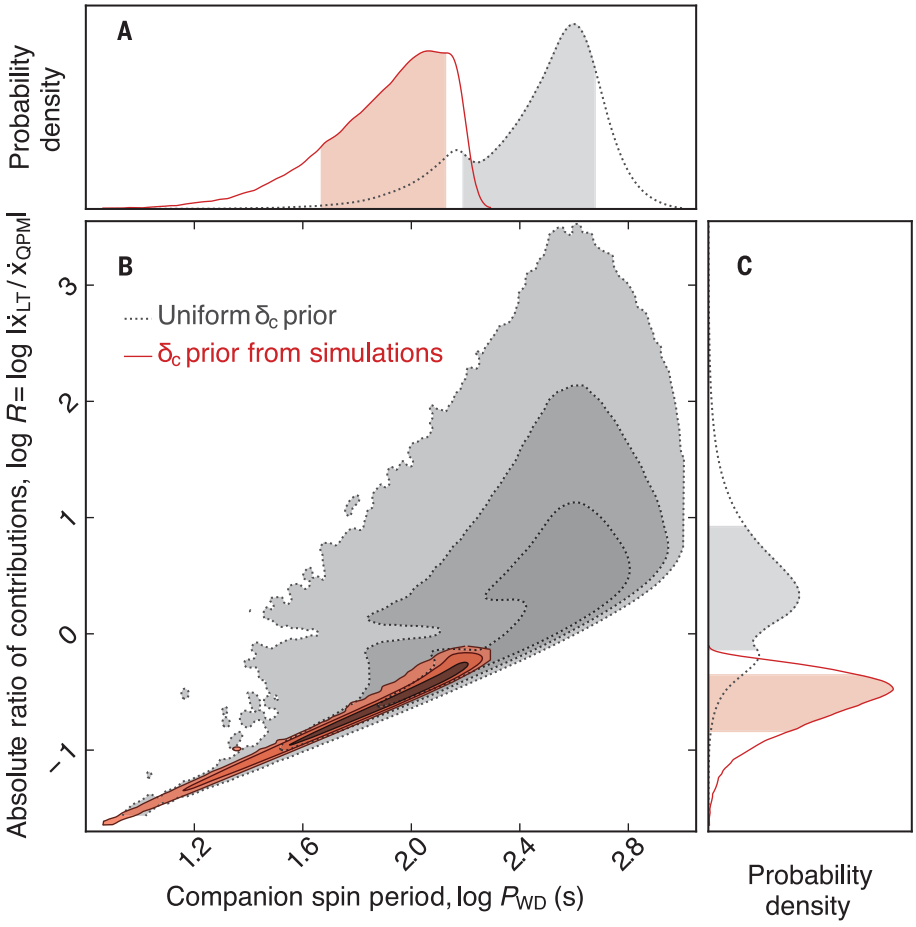

Fig. 2. Contributions to orbital precession from WD rotation. The absolute ratio of the contributions to $\dot{x}_{SO}$ from $\dot{x}_{LT}$ and $\dot{x}_{QPM}$, $R = |\dot{x}_{LT}/\dot{x}_{QPM}|$, is plotted as a function of P_{WD}. (**A** and **C**) Marginalized posterior distributions with their 68% confidence intervals shaded, defined as the combination of the two 34% confidence regions on either side of the 2D maximum of the likelihood function. (**B**) Two-dimensional probability distribution with contours defining the 68%, 95%, and 99% likelihood confidence intervals. The gray-shaded regions and dotted contours are constraints using only the radio observations of the pulsar, whereas the red regions and solid contours include additional binary evolutionary constraints from simulations (*8*). Numerical values are provided in Table 2.

and derived parameters of the system are provided in Table 1.

We measure the temporal evolution of x for this system, $\dot{x}_{obs} = (1.7 \pm 0.3) \times 10^{-13}$ s s^{-1}. This value may include contributions from different physical and geometric effects depending on whether there is a corresponding change in a_p, i, or A. We find (*8*) only two appreciable contributions to $\dot{x}_{obs}$: The largest is a change in i that is due to the precession of the orbital plane caused by the spin of the WD ($\dot{x}_{SO}$), with a smaller contribution arising from a change in A caused by geodetic precession of the pulsar (*10*). The magnitude of the latter contribution was computed from the precessional constraints on the system's geometry (*8*, *19*); we find that it contributes <21% of $\dot{x}_{obs}$ at 99% confidence. The remainder is caused by $\dot{x}_{SO}$, the largest contribution, which corresponds to an average increase of i of 1.7 arc sec per year. All other contributions are several orders of magnitude smaller (*8*).

Both QPM and LT effects induced by the WD spin (and only these effects) provide non-negligible contributions to $\dot{x}_{SO}$: The QPM contribution ($\dot{x}_{QPM}$) is inversely proportional to the square of the WD spin period (P_{WD}), whereas the LT contribution ($\dot{x}_{LT}$) is inversely proportional to P_{WD}. These effects also contribute to $\dot{\omega}$, but for this system the contribution is expected to be smaller than our observational uncertainties. The LT contribution to $\dot{\omega}$ is potentially detectable in compact double-NS systems such as the double pulsar, PSR J0737–3039A (*22*).

Both $\dot{x}_{QPM}$ and $\dot{x}_{LT}$ are modulated by the spin misalignment angle (δ_c) and the precession phase (Φ_c^0; see Fig. 1) of the WD at our reference epoch (T_0; see Table 1). Both of these angles are unknown, so we performed Markov Chain Monte Carlo (MCMC) computations to obtain a distribution for the individual contributions and used Bayesian statistics to marginalize over the parameter space of δ_c and Φ_c^0. From this, we infer the maximum allowable P_{WD} consistent with the observed $\dot{x}_{obs}$ (*8*).

Figure 2 shows the absolute ratio of the contributions from $\dot{x}_{LT}$ and $\dot{x}_{QPM}$, $R = |\dot{x}_{LT}/\dot{x}_{QPM}|$, as a function of P_{WD} (fig. S2 shows a full correlation plot). This demonstrates that we can constrain $P_{WD} < 900$ s with 99% confidence. For known isolated WDs, their spin periods are known to range from a few hours to a few tens of hours (*23*, *24*); the fastest rotating isolated WD known (SDSS J0837+1856), which also has a mass similar to the WD in the PSR J1141–6545 system [~0.9 solar masses ($M_\odot$)], has a spin period of ~1.13 hours (*24*). Our upper limit on P_{WD} is thus a confirmation of WD spin-up caused by an earlier episode of mass transfer. If $P_{WD} > 270$ s, LT is the dominant contributor to $\dot{x}_{SO}$. R never reaches zero (see also fig. S2), so for all allowed values of $\{\delta_c, \Phi_c^0\}$, $\dot{x}_{LT}$ never vanishes. Thus, we detect the action of LT drag in the motion of this binary pulsar.

Taking these results as confirmation of the evolutionary history discussed above, we use binary evolution simulations to constrain δ_c and place further constraints on P_{WD} (*8*). We find that the mass-transfer phase lasts for ~16,000 years before the resulting pulsar progenitor star undergoes an "ultrastripped" SN event (*25*–*27*). If the mass-accretion rate of the ~1.02 $M_\odot$ WD is restricted by the Eddington limit (i.e., the maximum rate of accretion before photon pressure blocks further accretion), which is ~4×10^{-8} $M_\odot$ per year for this WD, then it would accrete ~0.06 $M_\odot$ in this time. We choose an initial orbital period and mass of the pulsar progenitor star to reproduce the most probable pre-SN binary parameters using 70 million simulations of post-SN orbital parameters of systems resembling PSR J1141–6545 (*8*).

These simulations allow us to estimate a lower limit on P_{WD} of ~20 s, although this depends on the interactions between the accreted material and the magnetosphere of the WD, which is not known. The angular velocity at which the WD would break up provides a firmer lower limit on P_{WD} of 7 s. The value of δ_c obtained from simulations is <50° at 99% confidence. This means that the WD spin is prograde, i.e., still rotating in the same

Table 1. Model parameters for PSR J1141–6545. Shown are postfitting model parameter values for PSR J1141–6545 with the DDGR timing model. The glitch parameters apply to a previously known pulsar glitch that occurred in 2008 (*8*).

Dataset and model fit quality	
Modified Julian date (MJD) range	51,630.8 to 58,214.5 (18.03 years)
No. of TOAs	20,861
Weighted root mean square timing residual (μs)	95.6
Reduced χ^2 value	1.0004
Fixed quantities	
Reference epoch (MJD)	54,000
Glitch epoch (MJD)	54,272.7
Measured quantities	
Right ascension, α (J2000 equinox)	$11^h41^m07.007^s \pm 0.003^s$
Declination, δ (J2000 equinox)	−65°45′19.14″ ± 0.1″
Pulse frequency, ν (s^{-1})	$2.5387230404 \pm 1 \times 10^{-10}$
First derivative of pulse frequency, $\dot{\nu}$ (s^{-2})	$-2.76800 \times 10^{-14} \pm 1 \times 10^{-19}$
Dispersion measure, DM (pc cm^{-3})	115.98 ± 0.03
Orbital period, P_b (d)	$0.19765096149 \pm 3 \times 10^{-11}$
Epoch of periastron, T_0 (MJD)	$53999.9960283 \pm 2 \times 10^{-7}$
Projected semimajor axis of orbit, x_{obs} (s)	$1.858915 \pm 3 \times 10^{-6}$
Longitude of periastron, ω_0 (degrees)	$80.6911 \pm 6 \times 10^{-4}$
Orbital eccentricity, e	$0.171876 \pm 1 \times 10^{-6}$
First derivative of x, $\dot{x}_{obs}$ (s s^{-1})	$(1.7 \pm 0.3) \times 10^{-13}$
First derivative of e, $\dot{e}$ (s^{-1})	$(-2 \pm 8) \times 10^{-15}$
Companion mass, M_c ($M_\odot$)	1.02 ± 0.01
Total mass, M_{TOT} ($M_\odot$)	$2.28967 \pm 6 \times 10^{-5}$
Glitch phase	1.0011 ± 0.0001
Glitch-induced step change in ν (Hz)	$(1.49508 \pm 0.0001) \times 10^{-6}$
Glitch-induced step change in $\dot{\nu}$ (Hz s^{-1})	$-(8.7 \pm 0.2) \times 10^{-17}$
Derived quantities	
Pulsar mass, M_p ($M_\odot$)	1.27 ± 0.01
Orbital inclination, i (degrees)	71 ± 2 or 109 ± 2

Table 2. Confidence intervals (68%) from Fig. 2. Shown are the 68% confidence intervals of the companion spin period and the absolute ratio of contributions to $\dot{x}_{SO}$ from $\dot{x}_{LT}$ and $\dot{x}_{QPM}$.

Parameter	Uniform δ_c prior	δ_c prior from simulations
Companion spin period [P_{WD} (s)]	397^{+78}_{-242}	116^{+17}_{-70}
Absolute ratio of contributions to $\dot{x}_{SO}$ [$R = |\dot{x}_{LT}/\dot{x}_{QPM}|$]	$2.13^{+6.18}_{-1.41}$	$0.33^{+0.11}_{-0.19}$

direction as the orbit (before the SN, the WD spin was most probably aligned with the orbit, $\delta_c \sim 0°$, caused by accretion of matter from the pulsar's progenitor). We use the distribution of δ_c from simulations as a prior for additional MCMC computations, obtaining tighter constraints for the distribution of R and P_{WD} shown in Fig. 2 (see also fig. S3 for a full correlation plot). We find that P_{WD} is <200 s with 99% confidence. This is because, for $\delta_c < 50°$, $\dot{x}_{QPM}$ is positive whereas $\dot{x}_{LT}$ is negative. To obtain the net positive $\dot{x}_{SO}$ that we observe, the WD needs to spin substantially faster so the excess from QPM ($\dot{x}_{QPM} - \dot{x}_{SO}$) compensates for the negative $\dot{x}_{LT}$. Table 2 provides the 68% confidence limits on R and P_{WD} with and without binary evolution simulations. These WD spin constraints correspond to an angular momentum between 2 and 20×10^{48} g cm^2 s^{-1}. This is one to two orders of magnitude larger than the range observed among the recycled pulsars in double-NS systems, 0.03 to 0.4×10^{48} g cm^2 s^{-1}, which also likely experienced accretion onto the first-formed NS (*26*).

In summary, measurement of the relativistic effects in the PSR J1141–6545 system have enabled us to determine the masses of its WD and NS components, the orbital inclination, and its variation. This variation is dominated by contributions from both the Newtonian quadrupole spin–orbit coupling and the LT precession caused by the rapidly spinning WD. LT precession is required for any orbital orientation and is the dominant term if $P_{WD} >$ 270 s after marginalizing over the system's geometry. For prograde rotation of the WD, which is indicated by binary evolution simulations, $P_{WD} < 200$ s and LT precession has an opposite sign to the quadrupolar term. PSR J1141–6545 therefore exhibits another manifestation of Einstein's general theory of relativity: LT frame dragging.

REFERENCES AND NOTES

1. I. Ciufolini, J. A. Wheeler, *Gravitation and Inertia* (Princeton Univ. Press, 1995).
2. J. Lense, H. Thirring, *Phys. Z.* **19**, 156 (1918).
3. I. Ciufolini, E. C. Pavlis, *Nature* **431**, 958–960 (2004).
4. C. W. F. Everitt *et al*., *Phys. Rev. Lett.* **106**, 221101 (2011).
5. C. S. Reynolds, *New Astron.* **3**, 41–47 (2019).
6. N. Wex, *Class. Quantum Gravity* **12**, 983–1005 (1995).
7. V. M. Kaspi, M. Bailes, R. N. Manchester, B. W. Stappers, J. F. Bell, *Nature* **381**, 584–586 (1996).
8. Materials and methods are available as supplementary materials.
9. D. R. Lorimer, M. Kramer, *Handbook of Pulsar Astronomy* (Cambridge Univ. Press, 2012).
10. T. Damour, J. H. Taylor, *Phys. Rev. D Part. Fields* **45**, 1840–1868 (1992).
11. T. Damour, N. Deruelle, *Ann. Inst. Henri Poincaré Phys. Théor.* **43**, 107–132 (1985).
12. T. Damour, N. Deruelle, *Ann. Inst. Henri Poincaré Phys. Théor.* **44**, 263–292 (1986).
13. V. M. Kaspi *et al*., *Astrophys. J.* **543**, 321–327 (2000).
14. J. Antoniadis, C. G. Bassa, N. Wex, M. Kramer, R. Napiwotzki, *Mon. Not. R. Astron. Soc.* **412**, 580–584 (2011).
15. T. M. Tauris, T. Sennels, *Astron. Astrophys.* **355**, 236 (2000).
16. R. P. Church, S. J. Bush, C. A. Tout, M. B. Davies, *Mon. Not. R. Astron. Soc.* **372**, 715–727 (2006).
17. B. M. Barker, R. F. O'Connell, *Phys. Rev. D Part. Fields* **12**, 329–335 (1975).
18. A. W. Hotan, W. van Straten, R. N. Manchester, *Astron. Soc. Aust.* **21**, 302–309 (2004).
19. V. Venkatraman Krishnan *et al*., *Astrophys. J.* **873**, L15 (2019).
20. M. Bailes *et al*., *Astron. Soc. Aust.* **34**, e045 (2017).
21. J. H. Taylor, J. M. Weisberg, *Astrophys. J.* **345**, 434 (1989).
22. M. S. Kehl, N. Wex, M. Kramer, K. Liu, in *Fourteenth Marcel Grossmann Meeting–MG14* (2018), pp. 1860–1865.
23. S. D. Kawaler, in *19th European Workshop on White Dwarfs*, P. Dufour, P. Bergeron, G. Fontaine, eds. (2015), vol. 493 of *Astronomical Society of the Pacific Conference Series*, p. 65.
24. J. J. Hermes *et al*., *Astrophys. J.* **841**, L2 (2017).
25. T. M. Tauris *et al*., *Astrophys. J.* **778**, L23 (2013).
26. T. M. Tauris, N. Langer, P. Podsiadlowski, *Mon. Not. R. Astron. Soc.* **451**, 2123–2144 (2015).
27. K. De *et al*., *Science* **362**, 201–206 (2018).
28. V. Venkatraman Krishnan *et al*., Data and software release for: Lense–Thirring frame dragging induced by a fast-rotating white dwarf in a binary pulsar system, Zenodo (2019); https://doi.org/10.5281/zenodo.3555380.

ACKNOWLEDGMENTS

We thank the referees and the editor for a thorough reading of the manuscript and for suggesting helpful improvements; J. Antoniadis, M. Kramer, L. Lentati, D. Reardon, R. M. Shannon, and S. Stevenson for discussions on this paper; N. Langer for the use of his binary evolution (BEC) code; and L. Toomey, J. Hurley, and E. Ali for help with the data release. Data reduction and analysis were performed on the gSTAR and OzSTAR national supercomputing facilities at Swinburne University of Technology. This research has made extensive use of NASA's Astrophysics Data System (https://ui.adsabs.harvard.edu/) and includes archived data obtained through the CSIRO Data Access Portal (http://data.csiro.au). **Funding:** This research was primarily supported by the Australian Research Council Centre of Excellence for All-sky Astrophysics (CAASTRO; project no. CE110001020). The gSTAR and OzSTAR supercomputers are funded by Swinburne and the Australian Government's Education Investment Fund. V.V.K., N.W., and P.C.C.F. acknowledge continuing support from the Max Planck Society. M.B., C.F., and S.O. acknowledge Australian Research Council grants OzGrav (CE170100004) and a laureate fellowship (FL150100148). P.C.C.F. acknowledges financial support from the European Research Council (ERC) starting grant BEACON (contract no. 279702). T.M.T. acknowledges an AIAS–COFUND Senior Fellowship funded by the European Union's Horizon 2020 Research and Innovation Programme (grant no. 754513) and the Aarhus University Research Foundation. P.A.R. acknowledges support from the Australian Research Council (Discovery Project no. DP140102578). N.D.R.B. acknowledges support from a Curtin Research Fellowship (CRF12228). The Parkes radio telescope is funded by the Commonwealth of Australia for operation as a National Facility managed by CSIRO. The Molonglo Observatory is owned and operated by the University of Sydney with support from the School of Physics and the University. **Author contributions:** V.V.K. led the analysis; wrote software for data reduction, analysis, and interpretation; and led writing of the manuscript. V.V.K., M.B., W.v.S., and N.D.R.B. performed all observations with the Parkes telescope. V.V.K., M.B., C.F., A.J., and S.O. performed all observations with the UTMOST telescope. V.V.K, W.v.S., and S.O. performed robust polarization calibration and profile evolution modeling. V.V.K, E.F.K., and P.A.R. performed bootstrap ToA analysis and red noise modeling. V.V.K., M.B., N.W., and P.C.C.F. interpreted the results and analyzed precessional contributions to the observed values. T.M.T. performed and interpreted the binary evolution and SN simulations. **Competing interests:** The authors declare no competing interests. **Data and materials availability:** Our observational data and analysis software, including links to the software dependencies and each observational dataset, are available at Zenodo (*28*).

SUPPLEMENTARY MATERIALS

science.sciencemag.org/content/367/6477/577/suppl/DC1
Materials and Methods
Supplementary Text
Figs. S1 to S11
Table S1
References (*29*–*64*)

10 May 2019; accepted 3 December 2019
10.1126/science.aax7007